DIAGNOSTICS OF CLOUD-RADIATION INTERACTIONS USING MODEL-SIMULATED METEOSAT BRIGHTNESS TEMPERATURES

Jean-Jacques Morcrette

European Centre for Medium range Weather Forecasts
Shinfield Park, Reading, U.K.

Abstract

Brightness temperatures in the longwave window channel of METEOSAT are simulated from cloudiness, temperature and humidity fields produced by the forecast model, and compared to the equivalent ISCCP B3/CX observations over a 5 days period in July 1983.

Over some limited 10 x 10 deg^2 areas, representative of different cloud régimes, cloudiness is retrieved using cumulative frequency distributions of the window brightness temperature. Model diagnosed cloudiness is then compared to cloudiness retrieved from either observed or model-simulated brightness temperatures.

Results emphasize the need for validating the radiative impact of the clouds more than the cloud cover itself in a NWP model. Introduction of a *model simulated* time and area dependent threshold is shown to greatly improve the retrieval of a cloud cover over land.

1. INTRODUCTION

Experiments by Albrecht et al. (1986), Slingo and Slingo (1988), and Randall et al. (1989) have demonstrated the intricate interactions between moist processes, clouds and radiation. The latter two papers particularly show that, in the tropics, the effects of clouds make the radiative contribution a sizeable part of the total diabatic heating. As the tridimensional distribution of diabatic heating in the tropics is known to influence the circulation in the extratropics with a one to two weeks time lag (Tiedtke, 1984), it is relevant in the context of a numerical weather prediction model to assess the quality of the representation of the cloudiness and of its response to the diurnal cycle of insolation, as any deficiency in the interactions between moist processes, cloudiness and radiation in the tropics is likely to affect the quality of the forecasts.

The validation of the cloudiness forecast by a large-scale atmospheric

model through comparisons with observations is a difficult exercise, due to problems inherent to the retrieval of an "observed" cloudiness from satellite observations of radiances (Slingo, 1987). Model cloudiness is characterized by cloud parameters such as fractional cover, cloud-top temperature and cloud emissivity. These can be either diagnosed or prognosed via a cloud generation scheme.

In the context of a NWP model, the direct comparison of observed and model simulated brightness temperatures may be more consistent and fruitful than trying to compare model diagnosed and satellite-derived cloudiness. Although the latter comparisons are certainly valuable, the "model-to-satellite approach" advocated by Morcrette (1991) minimizes the uncertainties due to potentially different assumptions (regarding for example cloud optical properties or surface emissivity) in the cloud retrieval scheme and the model radiation scheme. This is specially true if the same radiation scheme is used both for simulating the diagnostic radiances and for computing the radiative heating rates required by the model's thermodynamic equation. Moreover, this approach makes provision for a consistent use of radiance measurements from geostationary satellites *on a real time basis* inasmuch as all necessary diagnostics are produced on the model side and do not rely on external satellite data processing the results of which might be available only in a delayed mode. Furthermore, this approach can be applied whatever the horizontal resolution of the satellite measurements and the model outputs. Finally, the emphasis put on the evaluation of the radiative impact of the clouds more than of the clouds themselves is consistent with the cloud forcing approach, extensively used in the recent work performed with ERBE (Earth Radiation Budget Experiment) measurements (Ramanathan et al., 1989).

In this paper, we illustrate the very difficulty of comparing the cloud cover computed by the model cloud scheme with a retrieved cloud cover, and show that more information provided by a model can help a retrieval scheme. Section 2 briefly discusses the methodology of the study. In section 3, we apply a simple threshold technique to the cumulative frequency distribution of the observed and computed T_B to retrieve a cloudiness estimate. We illustrate the large impact of using a fixed vs. a time and area dependent threshold. We show that, even given the imperfections in the various physical parameterizations of the ECMWF model, a *threshold computed from model simulated clear-sky brightness temperatures* helps improve the retrieval of a cloud cover even if using longwave window channel radiance measurements only.

2. METHODOLOGY

The details of the computations of the synthetic METEOSAT longwave window channel radiances from the temperature, humidity and cloudiness profiles produced by the model are given in Morcrette (1991). The limitations and uncertainties linked to the "model-to-satellite" approach are also discussed in some details in that paper. Results presented hereafter are for a 5-day simulation from 3 July 1983, 12Z, carried out with the CY36 version of the operational model.

We have used the ISCCP-B3 radiance data (Schiffer and Rossow, 1985) over the area 67.5 °N- 67.5 °S, 67.5 °W - 67.5 °E, corresponding roughly to the field of view of METEOSAT. The calibrated radiance or equivalent brightness temperature T_B in the 10.5 - 12.5 μm channel is given every three hours (at 0000, 0300, ... 2100 GMT). In order to have similar spatial resolution for both satellite observations and model outputs, the observed T_B (representative of about $(30\ km)^2$ areas at nadir) are degraded to the T106 resolution of the current ECMWF forecast model. We also use the B3 radiances to retrieve a cloud cover that is compared in section 2 to a cloud cover present in the so-called ISCCP CX pilot data set. This early pilot data set was made available to various groups early 1986 to evaluate the results of an early test version of the ISCCP cloud algorithm. We use this data set as it is the only available to us including cloud parameters at the same resolution as the B3 radiance data. It must be noticed that the cloud parameters present in this CX data set can be very different from the final ISCCP C1 products derived with a much improved algorithm, but available only at the $2.5^\circ \times 2.5^\circ$ resolution, which we consider less relevant to our purpose of validating the cloudiness produced by a high-resolution forecast model.

Eleven limited areas (10.125 x 10.125 deg^2, corresponding to 9 x 9 T106 grid boxes) were finally defined, over which we have concentrated our study. Characteristics of these areas are given in Table 1. Over these limited areas, the diurnal variations of the cloudiness and related brightness temperature as seen in the METEOSAT measurements and as produced in the model are studied using normalized cumulative frequency distributions of the observed T_B [hereafter referred to as CFD (T_B)] for retrieving an observed cloud fraction over the limited areas for comparison with the model cloudiness.

Table 1: Characteristics of the eleven limited areas

N	Geographical location	Latitude	Longitude	Main features
1	Newfoundland Basin	51N-41N	45W-35W	N.H. frontal systems
2	Egypt, Libya	29N-19N	20E-30E	clear-sky desert
3	Cape Verde Island	26N-16N	28W-18W	Stratiform clouds
4	Mauritania, Mali	20N-10N	15W- 5W	convection over land
5	Niger, Nigeria	20N-10N	5W- 5E	convection over land
6	Sierra Leone Basin	16N- 6N	34W-24W	convection over ocean
7	Ethiopia	15N- 5N	31E-41E	convection over land
8	Central Africa	8N- 2S	21E-31E	convection over land
9	Off-coast Angola	7S-17S	0E-10E	Stratiform clouds
10	Central Mid-Atlantic	10S-20S	26W-16W	trade-wind Cu clouds
11	Gough Island	39S-49S	16W- 6W	S.H. frontal systems

Ruprecht et al. (1987) show that cumulative frequency distributions of T_B offer a simple and convenient way to retrieve the fractional cloudiness over an area: Given the mean surface brightness temperature T_{Bs} and a brightness temperature threshold ΔT_B (incorporating the effect of surface temperature inhomogeneities), all observed T_B's below $T_{Bs} - \Delta T_B$ are assumed to stem from cloudy pixels within the studied area, so that

$$CF = 1 - CFD\ (T_{Bs} - \Delta T_B) \qquad (1)$$

is the fractional cloud cover. The main advantage of this method is that uncertainties in the threshold value are directly translated into uncertainties in the cloud fractional cover. On the other hand, different values for ΔT_B could allow one to differentiate between low-, medium- and high-level cloudiness. In principle, this method is best suited to retrieve the cloudiness over a homogeneous surface, i.e., the ocean, and it provides its best results when applied to both longwave window channel brightness temperatures and visible channel albedoes. For example, Ruprecht et al. (1987) have used this method to derive the cloud cover over the Atlantic Ocean from METEOSAT and GOES data. In their study, the thresholds were automatically

derived from the data themselves: the first relative minimum of the slope CFD (T_B) = f (T_B) is a good indicator of the separation between surface and clouds. Given our objective of comparing satellite-derived and model-generated cloudiness and associated T_B's and of using the two data sets as consistently as possible, we tested the effect of both a fixed ΔT_B and a variable threshold determined from model simulations over all areas, whether oceanic or continental (see section 3).

Morcrette (1991) discusses the problem of the potential loss of information when averaging the satellite to the model resolution, the accuracy of the radiation scheme used to compute the model-generated radiances, the quality of the inputs (surface temperature, humidity profile) to the radiation scheme and the impact of the uncertainties in the simulated clear-sky radiances, and the uncertainties in the retrieved clear-sky observations.

3. COMPARISON OF SATELLITE-DERIVED, MODEL-GENERATED AND RADIATIVELY EFFECTIVE MODEL CLOUDINESS

Figures 1 present, over the 8 most significant limited areas, the total cloudiness forecast by the model and the results of the *early pilot* ISCCP algorithm (as of mid-1986). On an instantaneous and on a pixel basis, the algorithm sorts out the B3 pixels in four categories: cloud, mixed, unclassified, and surface. In Figs. 1, the area between the zero line and the first line (thin full line with open squares) represents the fraction of pixels confidently identified as CLOUD; between that first line and the second one (dash line with full circles) are the pixels corresponding to a MIXED scene, covered with either sub-grid scale and/or semi-transparent clouds; then, between that second line and the third one (dotted line with open lozenges) can be found the pixels that this particular version of the ISCCP algorithm could not classify with certainty (UNCLASS); finally, the fraction between the third line and the top line (dot dash) represents the fraction of pixels sorted out with certainty as SURFACE, i.e. clear-sky, pixels by the ISCCP algorithm. Therefore the CLOUD fraction retrieved by the ISCCP algorithm should be seen as the minimum cloud fraction present over the area, and the third line (CLOUD + MIXED + UNCLASS) can be seen as defining the maximum cloud fraction present over the area, if we assume that all MIXED pixels are in fact semi-transparent clouds and that all UNCLASS pixels are cloudy pixels with pathological radiative characteristics (from the point of view of the ISCCP classification algorithm). Given these lower and upper limits for cloudiness,

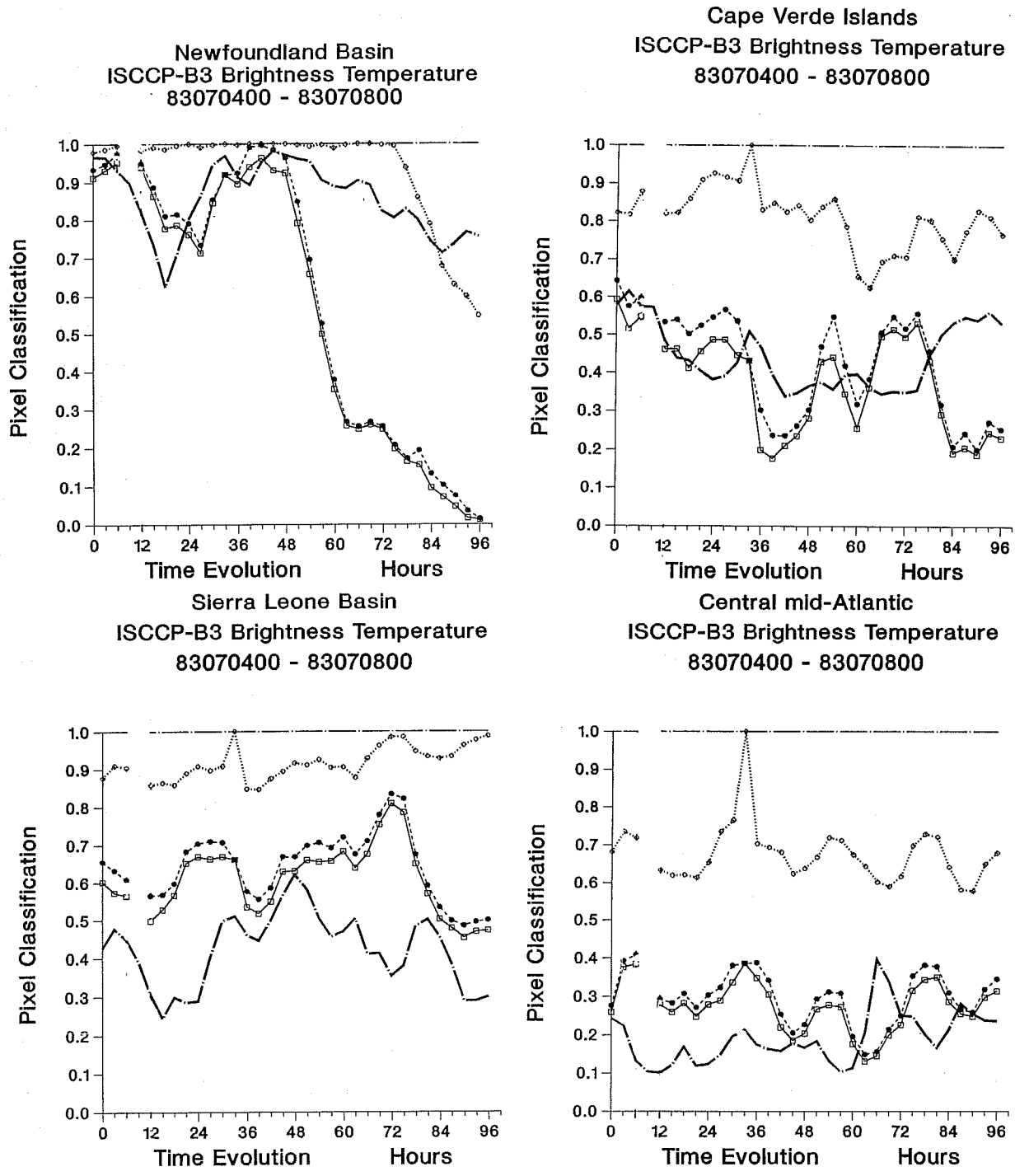

Fig. 1a) The total cloud cover diagnosed by the model (thick dot-dashed line) and the results of the ISCCP pilot pixel classification algorithm between 4 July 1983, 00GMT and 8 July 1983, 00GMT. Fraction of the pixels classified as cloud is below the full line with squares. Fraction of the pixels classified as mixed is between that full line and the dashed line with black circles. Fraction of the pixels not classified by the ISCCP pilot algorithm is between that dashed line and the dotted line with open lozenges. Fraction of the pixels classified as surface (i.e. clear-sky) is between that dotted line and the thin dot-dashed line at the top.

Over 4 oceanic areas; Newfoundland, Cape Verde Island, Sierra Leone Basin and Central Mid-Atlantic areas.

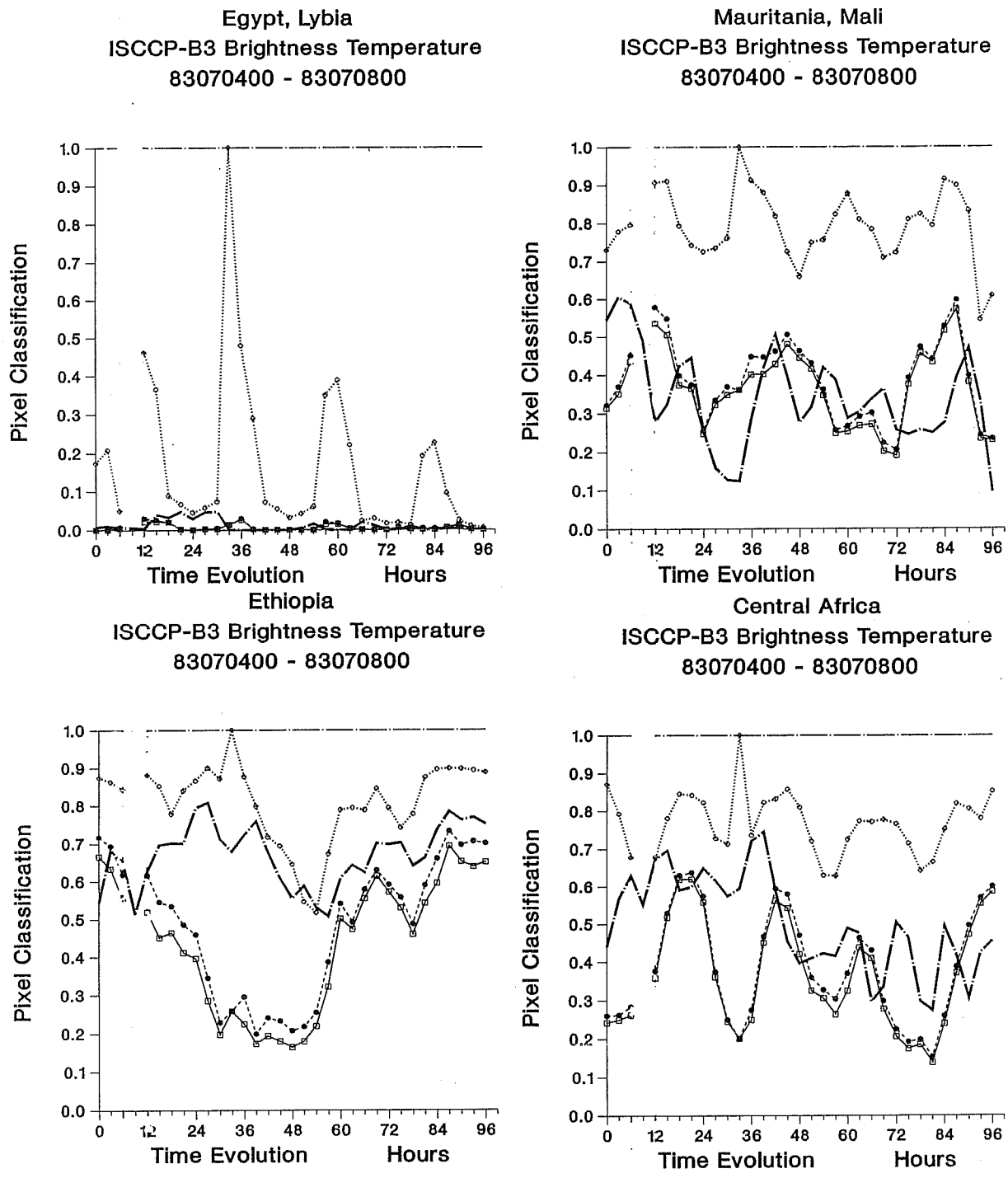

Fig. 1b) As fig. 1a) but over 4 land areas: Egypt-Libya, Mauritania-Mali, Ethiopia and Central Africa areas.

a qualitative assessment of the quality of model diagnosed cloudiness can be carried from Figs. 1. This comparison can only be qualitative as the range of uncertainty in the retrieved cloudiness is generally as high as 40 percent. The corresponding total cloudiness given by the ISCCP algorithm in the different limited areas averaged over the four days are given in Table 2.

Over the ocean (Fig. 1a), the model underestimates the average cloudiness over most areas relative to the lower limit (the CLOUD line). This underestimation is particularly obvious over the Sierra Leone Basin (by 18 %), off-coast Angola (by 9 %) and in the Central mid-Atlantic area (by 9 %). In the frontal areas, the model overestimates the cloudiness over the Newfoundland Basin, mainly due to an improper location of a storm system after 3 forecast days. Over the Gough Island area, the model underestimates the cloudiness (by 13 %) but captures more of the variability of the cloud cover.

Over land (Fig. 1b), the agreement on the average level of cloudiness (MODEL vs. CLOUD) is rather good over Egypt-Libya, Mauritania-Mali, Niger-Nigeria (better than 5 %). Over the Ethiopian and Centrafrican areas, the model diagnosed cloudiness lies between the lower and upper limits that has been derived from the satellite observations by the ISCCP algorithm. However, this agreement is very relative as the range of uncertainty in the retrieved cloudiness is very large. Moreover, inferring any useful information on the quality of the diurnal variability of the model cloudiness on a regional basis but on such a short time scale is unrealistic. In all areas, except off-coast Angola, adding the fraction of MIXED pixels to the fraction of CLOUD pixels increases the cloud cover by less than 5 %.

At this point, it is interesting to study how it would be possible to improve the retrieval of a cloud cover from the satellite observations to make these comparisons with model cloudiness less uncertain then more meaningful.

The CFD (T_{Bo}), built from the full resolution ISCCP B3 T_{Bo}, have been used to retrieve a cloud cover from the ISCCP B3 observations. Over the ocean (land), a 3 K (6 K) threshold, similar to the ones used in this version of the ISCCP algorithm (Rossow et al., 1988), is assumed to account for the possible inhomogeneities in sea (land) surface temperature. Then, an "observed" cloudiness is obtained from the observed T_{Bo} by applying (1), taking for T_{Bos} the mean over the period of study of the warmest T_{Bo}. However, over land, the inhomogeneities in surface properties (longwave emissivity, surface thermal and hydrological resistances) and the resulting modulation with time of the width of the range of surface T_{Bo} makes very difficult the retrieval of a cloud cover using a fixed threshold. To evaluate the impact of the

Table 2: Time-averaged cloudiness over the limited areas as given from the model and the various retrievals. *Model* is the model diagnosed cloudiness, *cloud*, *+mixed*, *+unclass* refer to the cloud fractions obtained from the ISCCP algorithm classification, *Tm+fK*, *To+fK*, *Tm+vK*, and *To+vK* correspond to the cloudiness retrieved from the computed (*Tm*) or observed (*To*) brightness temperatures using a fixed (*fK*) or a model dependent (*vK*) threshold, respectively (see text). The model dependent threshold ΔT_{Bm} varies in the range given in the last column (in degress).

		ISCCP algorithm							
Area	Model	cloud	+mixed	+unclass	Tm+fK	To+fK	Tm+vK	To+vK	Range ΔT_{Bm}
1	0.857	0.566	0.590	0.935	0.706	0.802	0.615	0.651	2.0- 7.5
2	0.011	0.006	0.007	0.164	0.134	0.320	0.044	0.251	4.0-12.0
3	0.442	0.377	0.424	0.811	0.818	1.000	0.411	0.705	1.5- 4.5
4	0.347	0.365	0.384	0.791	0.672	0.772	0.461	0.386	7.5-22.5
5	0.262	0.283	0.295	0.655	0.537	0.693	0.380	0.316	5.5-24.0
6	0.426	0.607	0.642	0.916	0.765	1.000	0.610	0.823	2.0- 4.0
7	0.668	0.436	0.484	0.810	0.864	0.918	0.654	0.437	8.5-20.0
8	0.503	0.366	0.387	0.770	0.652	0.755	0.586	0.399	4.5-10.0
9	0.310	0.394	0.653	0.879	0.499	0.948	0.256	0.878	2.0- 3.5
10	0.189	0.273	0.297	0.675	0.585	0.725	0.461	0.383	2.0- 4.0
11	0.641	0.778	0.802	0.976	0.909	0.963	0.654	0.817	3.5- 8.5

uncertainties in the determination of the average clear-sky T_B over a given limited area, we have simply considered another value for ΔT_B namely the difference between the maximum and minimum clear-sky T_B's *simulated by the model* at a given time over a given limited area. This ΔT_{Bm} is the maximum range that model simulated T_{Bm} would show if all clouds were transparent over a given area.

To be consistent, we have also computed a similar cloudiness for the model from the model generated CFD (T_{Bm}) using the same two thresholds as applied on the observed T_{Bo}. Thus in Figs. 2a and c, we compare, for the oceanic and land areas respectively, the model cloudiness diagnosed from the cloud generation parameterization (Slingo, 1987), and the cloud cover retrieved from observed CFD (T_{Bo}) and computed CFD (T_{Bm}) using fixed

thresholds. In Figs. 2a and b, we similarly compare the model diagnosed cloudiness and the cloud cover retrieved from CFD (T_{Bo}) and CFD (T_{Bm}) using a time and area dependent threshold defined from the simulated range of clear-sky T_{Bm}. Total cloudiness as retrieved by these different methods and averaged over the 4 day period is given in Table 2.

The main result of these comparisons is that the use of a fixed threshold, even over the ocean, is inadequate. In Figs. 2a, a comparison of the model diagnosed cloudiness (the MODEL curve) and of the cloudiness retrieved from CFD (T_{Bm}) with a fixed ΔT_B of 3 K (the Tm+3K line) shows these two cloud covers are not consistent. The larger values for Tm+3K clearly indicates that the variability of the surface T_B, as simulated by the ECMWF model (recall that the sea surface temperature is prescribed from an NMC analysis of AVHRR longwave window measurements), is generally larger than 3 K, particularly at higher latitudes. The actual range of clear-sky T_{Bm} is presented in the last column of Table 2. When the threshold is defined as the range of T_B corresponding to the simulated clear-sky T_{Bm} (Figs. 3a), the agreement between the retrieved cloudiness (the Tm+DT line) and the model diagnosed cloudiness (the MODEL line) is much improved (see the first 48 h over Newfoundland Basin, or the Gough Island area for most of the period). However, when these two curves do not exactly correspond, it can be interpreted in terms of characteristics of the model clouds. For example, in areas where low stratiform should prevail (Cape Verde Islands and off-Coast Angola), a Tm+DT cloud cover smaller than the MODEL cloudiness indicates that the cloud is located very low in the atmosphere so that its longwave contrast relative to the T_{Bm} coming from the sea surface is often smaller than the range of sea surface T_{Bm} linked to SST variability. On the contrary, in areas where convective clouds are found (shallow convective clouds in the Central mid-Atlantic, and deeper convective clouds in the Sierra Leone Basin, the model dependent ΔT_{Bm} is in the 2 - 4 K range close to the fixed 3 K of the ISCCP algorithm (see Table 2); the ΔT_{Bm} appears too small to make the MODEL and Tm+DT clouds consistent.

Over land, the use of a fixed 6 K threshold has quite dramatic implications, which the most annoying is certainly the creation of some spurious diurnal variability in Tm+6K (but also To+6K). A closer look at the results for the Egypt-Libya area will illustrate the problem. For that area, where the actual cloudiness is small (MODEL is 1 %), Fig. 2b displays a large diurnal cycle of Tm+6K, which simply comes from the inhomogeneities of the surface properties producing a range of T_{Bm} larger than 6 K (up to 12 K

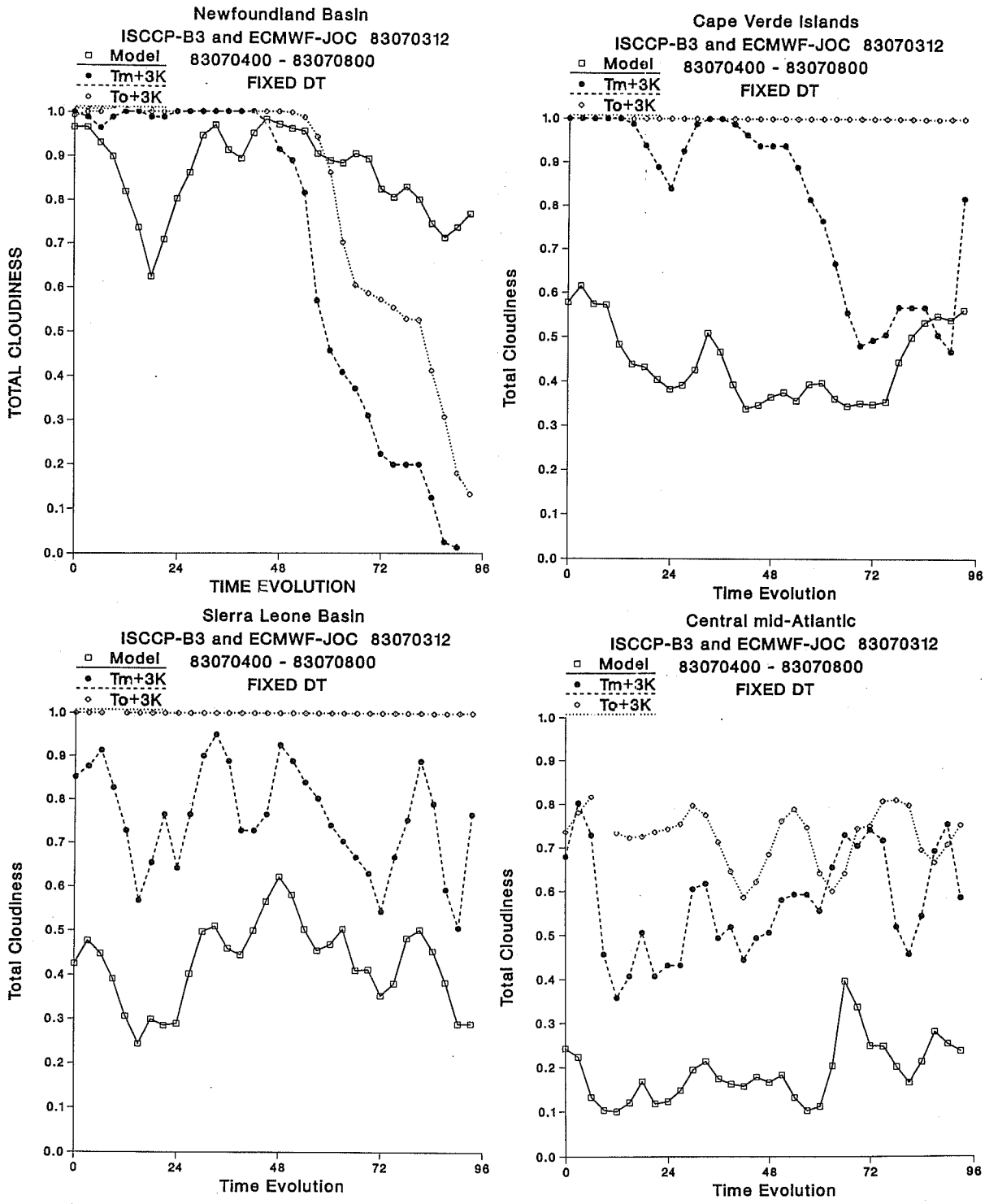

Fig. 2a) The total cloud cover diagnosed by the model (thick full line) and retrieved from the analysis of CFD of the observed T_B (dotted lines) and of the model generated T_B (dashed lines). Results are for the period between 4 July 1983, 00GMT and 8 July 1983, 00GMT. Analysis of the CFD (T_B) is performed for a fixed ΔT_B of 3 K over ocean areas and of 6 K over land areas.

Over 4 oceanic areas; Newfoundland, Cape Verde Island, Sierra Leone Basin and Central Mid-Atlantic areas.

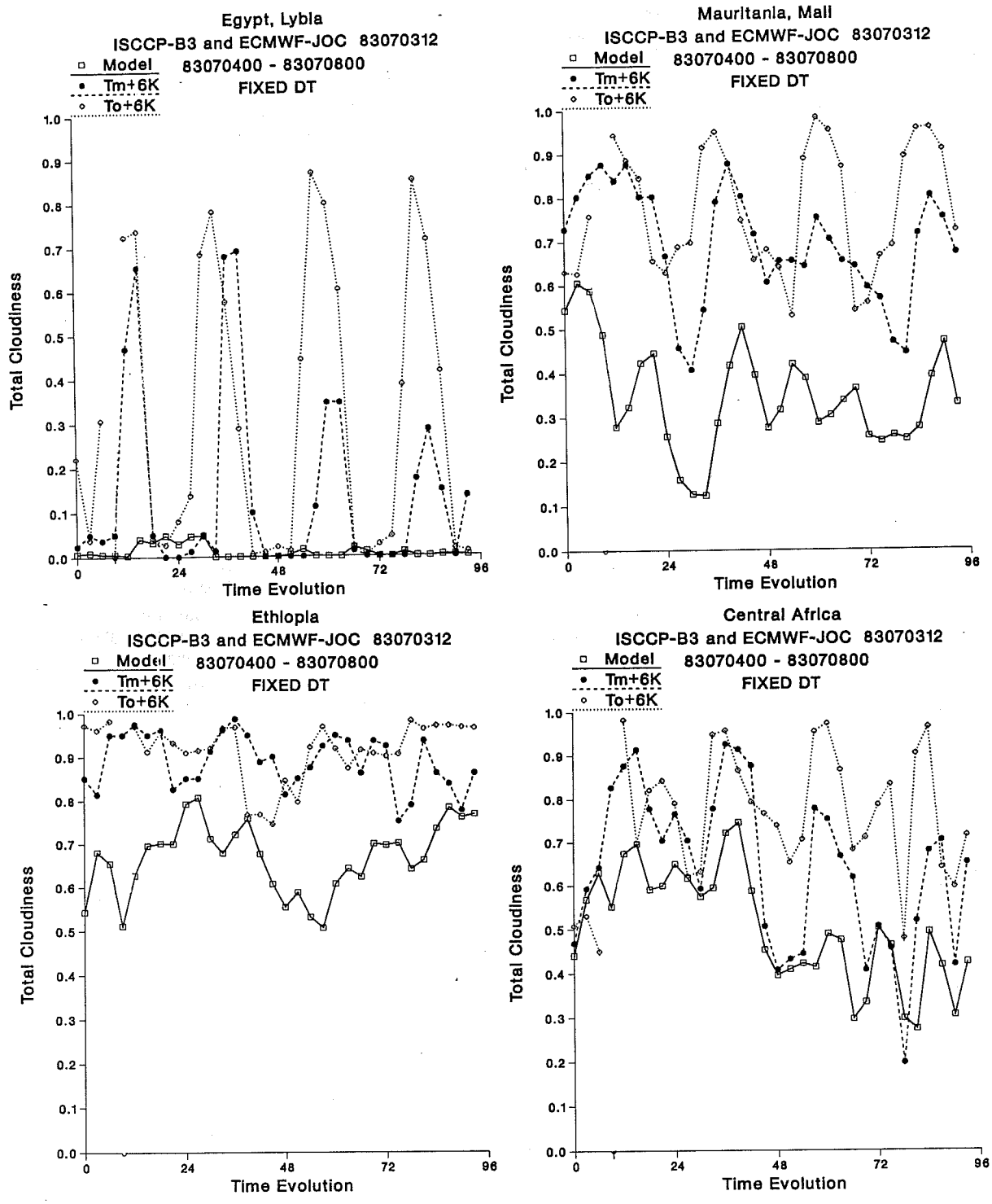

Fig. 2b) As fig. 2a) but over 4 land areas; Egypt-Libya, Mauritania-Mali, Ethiopia and Central Africa areas.

according to model simulations). When a model dependent ΔT_{Bm} is considered (Fig. 3b), this spurious cloudiness disappears. Similar features can be seen over all other land areas, except over Ethiopia where the high terrain and corresponding large precipitation in the model give a more complex pattern to the diurnal variability of surface temperature. With fixed threshold, the Tm+6K cloudiness is usually larger and presents more variability than the Tm+DT cloudiness.

The implication of using a fixed vs. a time and area dependent threshold cann also be seen when dealing with observed T_B. Comparisons of cloudiness retrieved from observations applying either a fixed 3 K (6K) or a model dependent ΔT_{Bm} to the CFD (T_{Bo}) show also large changes in retrieved cloudiness (see Table 2). The model dependent ΔT_{Bm} are generally larger than the 3 or 6 K fixed threshold and therefore give smaller cloud cover. It is also worthwhile to compare the results of these retrievals (To+3K with To+DT over the ocean, To+6K with To+DT over land) with the results of the ISCCP algorithm classification (Figs. 1a and b). Particularly interesting is the decrease in the number of unclassified pixels that a time and area dependent threshold seems to bring. In fact, the To+3K and To+6K cloudiness are generally in agreement with the CLOUD+MIXED+UNCLASS cloudiness (not quite as the ISCCP classification also relies on other parameters not accounted for in our approach, i.e., temporal and spatial coherence of both T_B and visible radiances) whereas the To+DT cloudiness is usually much closer to the CLOUD+MIXED cloudiness. This is particularly true, over the ocean, in the Newfoundland Basin, Central mid-Atlantic and Gough Island areas, and over land, over all areas except the clear-sky Egypt-Libya area. This clearly points out the negative role that a fixed threshold plays in giving a large number of unclassified pixels in this version if the ISCCP classification algorithm. Given that the ISCCP algorithm uses both the longwave window and visible channel measurements in its retrieval attempts, the improvement in decreasing the number of unclassified pixels through the use of a model simulated threshold applied on *only* longwave window measurements is really worth noticing.

4. Summary

The validation of the cloud fields produced by a NWP model on a few days time scale is made difficult by the large uncertainties in the cloudiness retrieved from satellite observations. We illustrate the large impact of using a fixed vs. a time and area dependent threshold. We show that, even given the

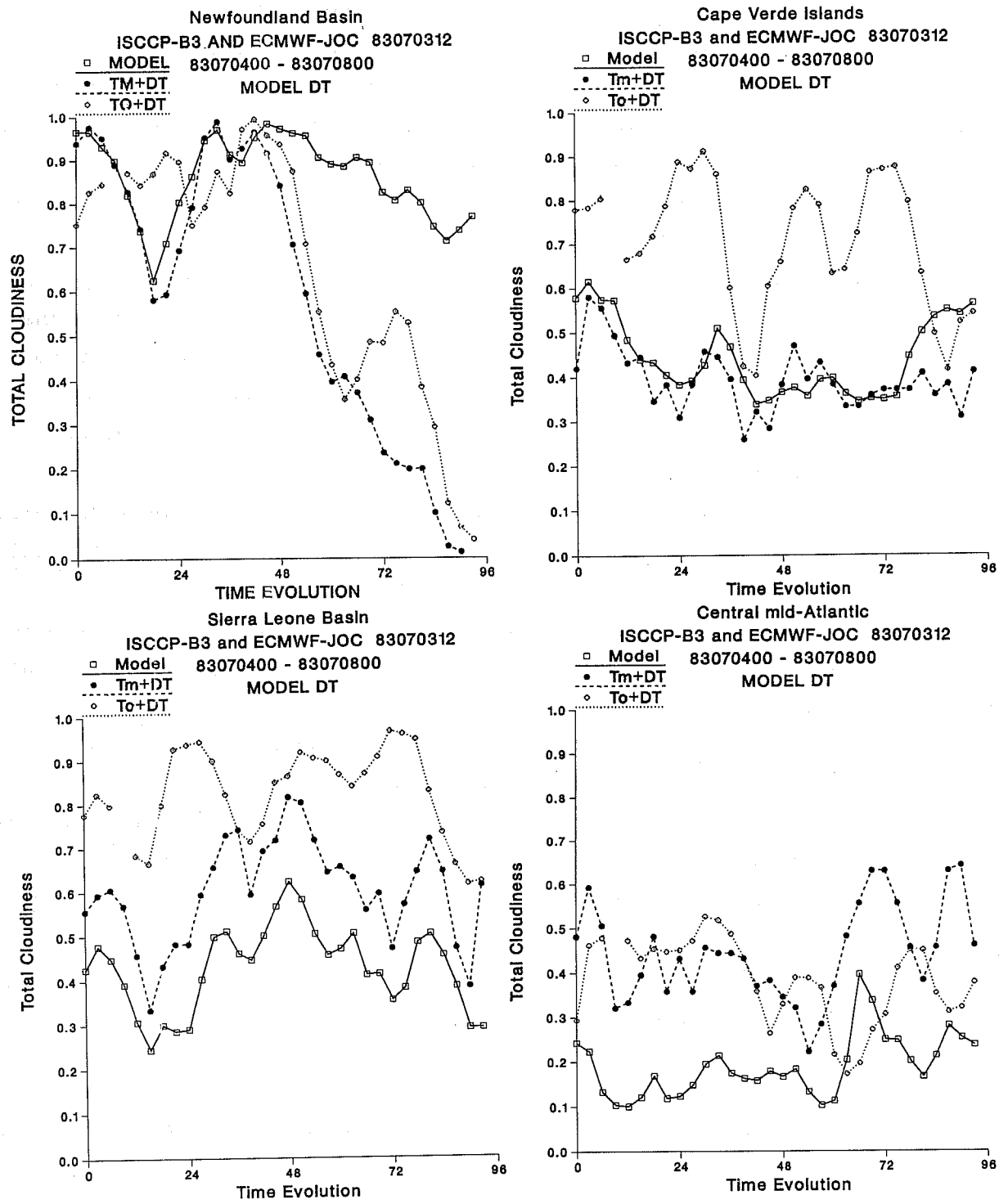

Fig. 3a) The total cloud cover diagnosed by the model (thick full line) and retrieved from the analysis of CFD of the observed T_B (dotted lines) and of the model generated T_B (dashed lines). Results are for the period between 4 July 1983, 00GMT and 8 July 1983, 00GMT. Analysis of the CFD (T_B) is performed for a model-dependent ΔT_B (see text).

Over 4 oceanic areas; Newfoundland, Cape Verde Island, Sierra Leone Basin and Central Mid-Atlantic areas.

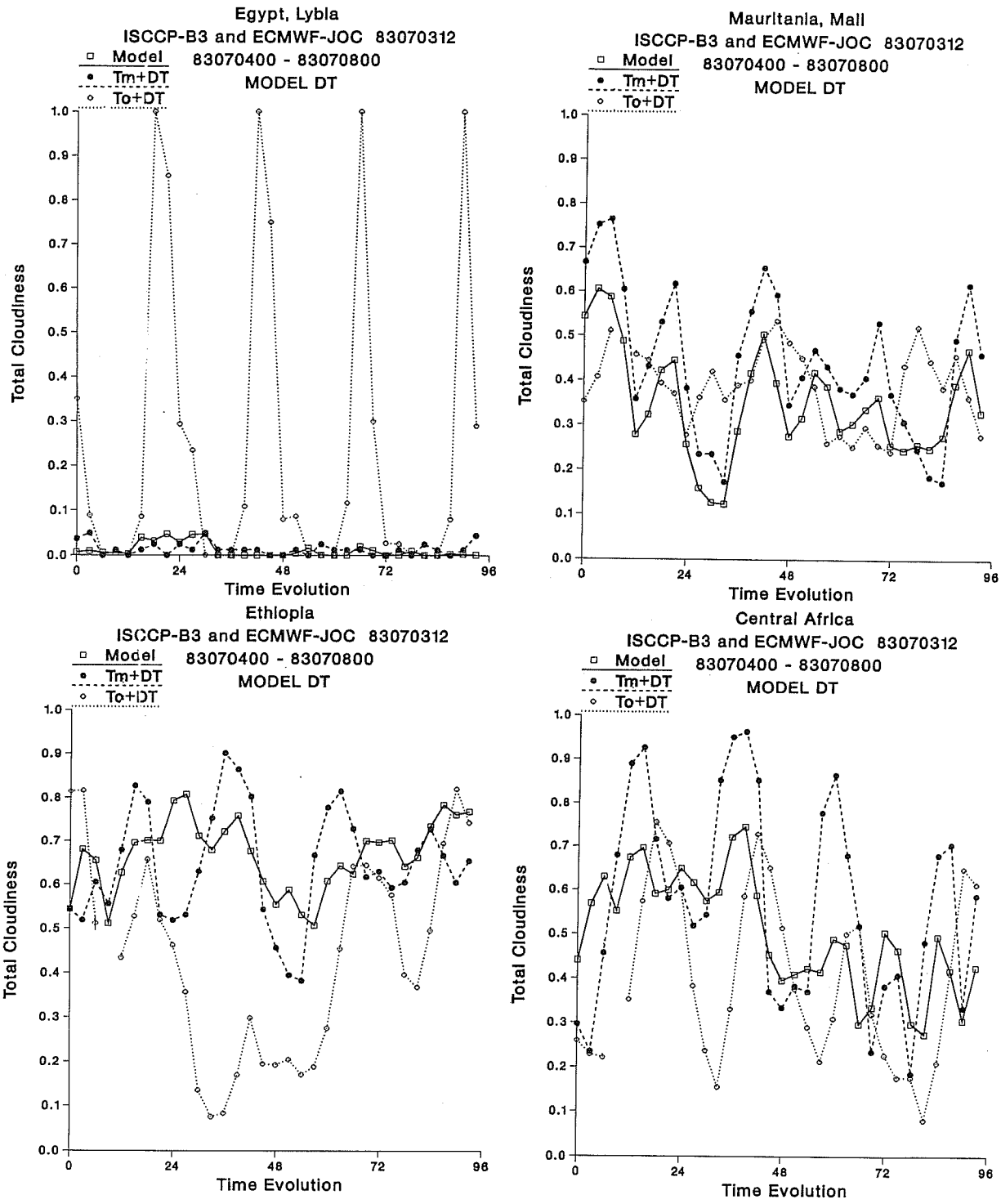

Fig. 3b) As fig. 3a) but over 4 land areas; Egypt-Libya, Mauritania-Mali, Ethiopia and Central Africa areas.

imperfections in the various physical parameterizations of the ECMWF model, a *threshold computed from model simulated clear-sky brightness temperatures* helps decrease the number of unclassified pixels. The use of such a variable threshold is likely to improve the retrieval of a cloud cover even if using longwave window channel radiance measurements only.

A similar study comparing observed and model-generated shortwave radiances would be very interesting. However, it is hindered by difficult problems related to the bi-directional reflectance properties of the surface and clouds, a surface albedo fixed at a mean annual value in the ECMWF model, and to the fact that shortwave radiances are more sensitive than the longwave ones to the details of the cloud microphysics (whereas bulk mass absorption coefficients are adequate to reproduce the effects of clouds on the longwave radiances).

Acknowledgments: Thanks are due to W. Rossow who clarified some points regarding the ISCCP pilot data set used in this study.

REFERENCES

Albrecht, B.A., V. Ramanathan, and B.A. Boville, 1986: The effects of cumulus moisture transport on the simulation of climate with a general circulation model. *J. Atmos. Sci.*, 43, 2443-2462.

Morcrette, J.-J., 1991: Evaluation of model-generated cloudiness: Comparison of satellite-observed and model-generated diurnal variability of brightness temperature. *Mon. Wea. Rev.*, **119**, in press, April issue.

Ramanathan, V., R.D. Cess, E.F. Harrison, P. Minnis, B.R. Barkstrom, E. Ahmad, and D. Hartmann, 1989: Cloud-radiative forcing and climate: Results from the Earth Radiation Budget Experiment. *Science*, 243, 57-63.

Randall, D.A., Harshvardhan, D.A. Dazlich, and T.G. Corsetti, 1989: Interactions among radiation, convection, and large-scale dynamics in a general circulation model. *J. Atmos. Sci.*, 46, 1943-1970.

Rossow , W.B., L.C. Garder, P.J. Lu, and A. Walker, 1988: International Satellite Cloud Climatology Project (ISCCP). Documentation of Cloud Data. WMO/TD-266, World Meteorological Organization, Geneva, Switzerland, 123 pp.

Ruprecht, E., E. Rudolph, and C. Simmer, 1987: Clouds over the Atlantic Ocean derived from the ISCCP B3 data of METEOSAT and GOES: A comparison. *Clouds in Climate II, WCRP workshop on Modeling and Observations*, Columbia, MD, Oct. 19-23, 1987, 42.

Schiffer, R.A., and W.B. Rossow, 1985: ISCCP Global Radiance Data Set: A new resource for climate research. *Bull. Amer. Meteor. Soc.*, 66, 1498-1505.

Slingo, J.M., 1987: The development and verification of a cloud prediction scheme for the ECMWF model. *Quart. J. Roy. Meteor. Soc.*, 113, 899-928.

Slingo, A., and J.M. Slingo, 1988: The response of a general circulation model to cloud longwave radiative forcing. I: Introduction and initial experiments. *Quart. J. Roy. Meteor. Soc.*, 114, 1027-1062.

Tiedtke, M., 1984: The effect of penetrative cumulus convection on the large-scale flow in a general circulation model. *Beitr. Phys. Atmosph.*, 57, 216-239.